



A model of solar radiation and Joule heating in magnetohydrodynamic (MHD) convective flow of thixotropic nanofluid



T. Hayat^{a,b}, M. Waqas^{a,*}, S.A. Shehzad^c, A. Alsaedi^b

^a Department of Mathematics, Quaid-I-Azam University, 45320, Islamabad 44000, Pakistan

^b Nonlinear Analysis and Applied Mathematics (NAAM) Research Group, Department of Mathematics, Faculty of Science, King Abdulaziz University, P.O. Box 80257, Jeddah 21589, Saudi Arabia

^c Department of Mathematics, Comsats Institute of Information Technology, Sahiwal 57000, Pakistan

ARTICLE INFO

Article history:

Received 29 November 2015

Accepted 1 January 2016

Available online xxxx

Keywords:

Hydromagnetics

Stagnation point flow

Thixotropic nanofluid

Joule heating

Viscous dissipation

Convective conditions

ABSTRACT

This paper reports the hydromagnetic stagnation point flow of thixotropic nanofluid towards an impermeable stretching surface. Effects of Brownian motion and thermophoresis are present. Heat and mass transfer analysis is performed in the presence of viscous dissipation, Joule heating and convective boundary conditions. Meaningful transformations are utilized to obtain nonlinear ordinary differential systems. Convergent solutions of the resulting differential systems are presented in series forms. Moreover the numerical values of skin friction coefficient, local Nusselt and Sherwood numbers are computed and analyzed.

© 2016 Elsevier B.V. All rights reserved.

1. Introduction

It is well known that sustainable energy generation is one of the most serious issues across the globe. Solar energy offers a solution with the hourly solar flux incident on the earth's surface being more prominent than the greater part of the human utilization of energy in a year. Concentrated solar energy has become the input for an increasing number of experimental and commercial thermal systems over the past few years. Recent studies indicated that the addition of nanoparticles to conventional working fluids (i.e., nanofluids) can improve heat transfer and solar collection. Solar energy is one of the best sources of renewable energy with minimal environmental impact [1]. Solar power is very important in our daily usage and it is a natural way of obtaining heat, electricity and water with the help from the nature. In the near future, we might be compelled to switch our controlling approaches to keep the aforementioned necessities. As we shall face some fossil fuels crisis the solar power is a renewable source of energy which never consumes. Power tower solar collectors are more effective through the use of nanofluid as a working liquid.

The use of nanoparticles is currently a subject of abundant studies. It is because of their Brownian motion and thermophoresis properties. A new class of heat transfer liquids is known as nanofluids (a base fluid and nanoparticles). The nanoparticles are used to improve the heat

transfer performance of the base liquids [2]. The cooling rate requirements cannot be obtained by the ordinary heat transfer liquids because their thermal conductivity is not adequate. Brownian motion of the nanoparticles enhances the thermal conductivity of base fluids. On the other hand, the magnetohydrodynamic (MHD) nanofluid has key significance in engineering, physics and chemistry. Particularly such liquids have wide scope in the optical switches, tunable optical fiber filters, optical grating, optical modulators, stretching of plastic sheets, polymer industry and metallurgy. Several metallurgical processes involve the cooling of continuous strips or filaments by drawing them through a nanofluid. Such strips in processes of drawing, thinning of copper wires and annealing are sometimes stretched. The quality and desired characteristics of a final product in such cases strongly depend upon the cooling rate by drawing such strips in an electrically conducting fluid. The magnetic nanoparticles are also useful in the construction of loudspeakers, magnetic cell separation, hyperthermia, drug delivery etc. MHD flow and radiation heat transfer of nanofluids in porous media with variable surface heat flux and chemical reaction are presented by Zhang et al. [3]. Sheikholeslami et al. [4] studied MHD CuO–water nanofluid with mixed convection. Influence of convective heat and mass conditions in MHD flow of nanofluid is reported by Shehzad et al. [5]. Abbasi et al. [6] studied the influence of heat and mass flux conditions in hydromagnetic flow of Jeffrey nanofluid. Numerical simulation of two phase nanofluid in the presence of time dependent magnetic field is addressed by Sheikholeslami et al. [7]. Recently Farooq et al. [8] examined the MHD Falkner–Skan flow of nanofluid.

* Corresponding author.

E-mail address: mw_qau88@yahoo.com (M. Waqas).

The phenomenon of non-Newtonian fluids has attracted the attention of recent researchers in view of several industrial and technological applications. Many materials such as toothpaste, paints, polymer solutions and melts, pharmaceuticals and chemical and biological liquids are examples of non-Newtonian fluids. These fluids show nonlinear relationship between the stress and the rate of strain which give rise to much complicated, more nonlinear and higher order differential systems. Despite all such complexities, several researchers are still engaged to examine the flows of non-Newtonian fluids under various aspects. Thus various models of non-Newtonian fluids have been suggested. Amongst these there is a thixotropic fluid model. The difference between thixotropic and shear thinning fluid is that a shear thinning fluid shows a decrease in viscosity with increasing shear rate while thixotropic fluid displays a decrease in viscosity over time at constant shear rate. Few studies relevant to thixotropic fluid can be seen in the refs. [9–12]. The stagnation point flow towards a stretching sheet commonly appeared in paper production, the spinning of fibers, glass blowing, continuous casting, manufacture of sheeting material through extrusion process especially in the polymer extrusion in a melt spinning process and aerodynamic extrusion of plastic sheets etc. Stagnation point flow of hydromagnetic viscous fluid over a stretching/shrinking sheet with generalized slip condition and homogeneous–heterogeneous reactions is studied by Abbas et al. [13]. Mabood et al. [14] examined MHD stagnation point flow with chemical reaction and transpiration. Malvandi et al. [15] analyzed the slip effects on unsteady stagnation point flow of nanofluid over a stretching sheet. Hayat et al. [16] investigated MHD stagnation-point flow of Jeffrey fluid over a convectively heated stretching sheet. Heat transfer analysis in unsteady boundary layer stagnation point flow towards a shrinking/stretching sheet is reported by Bhattacharyya [17].

Clearly Joule heating is produced due to the passage of electric current through any conducting material. It is because of the collision between the moving particles. In this process some of the kinetic energy is converted into the heat and as a result temperature of the body increases. In recent years the engineers and scientists are interested to increase the efficiency of various mechanical systems and industrial machineries. Such kinds of difficulties can be handled to decrease the temperature produced due to Ohmic dissipation or Joule heating. Therefore many researchers investigated the flow problems with various physical aspects. Effects of viscous dissipation and Joule heating in the MHD flow of second grade fluid past a radially stretching sheet with heat transfer is examined by Sahoo [18]. Hayat et al. [19] examined the effects of Joule heating and thermophoresis in flow over a stretched surface with convective boundary condition. MHD radiative stretched flow of Jeffrey fluid in the presence of Joule heating is reported by Shehzad et al. [20]. Hayat et al. [21] discussed the effects of Joule heating and thermal radiation in flow of third grade fluid over a radiative surface. Very recently Hayat et al. [22] studied MHD stagnation point flow of Jeffrey fluid by a radially stretching surface with viscous dissipation and Joule heating.

The aforementioned investigations witness that no attempt has been made to study the flow of thixotropic fluid in the presence of nanoparticles. Therefore our main objective is to explore the stagnation point flow of thixotropic nanofluid in the presence of viscous dissipation, Joule heating and convective conditions. Homotopic algorithm [23–30] is used for the development of solutions. Convergence of the obtained solutions is verified. Results for several sundry variables are examined.

2. Formulation

We consider the laminar hydromagnetic flow of an incompressible thixotropic nanofluid over a stretching sheet. The flow is induced due to the linear stretching of sheet. Thermophoresis and Brownian motion effects are taken into account. Magnetic field of strength B_0 is applied in transverse direction to the flow. Magnetic Reynolds number is taken small and thus the induced magnetic field is neglected. The flow analysis

is performed by considering the convective heat and mass conditions at the surface. Two-dimensional boundary layer flow equations are:

$$u \frac{\partial u}{\partial x} + v \frac{\partial v}{\partial y} = 0, \tag{1}$$

$$u \frac{\partial u}{\partial x} + v \frac{\partial u}{\partial y} = u_e \frac{du_e}{dx} + \frac{\sigma B_0^2}{\rho} (u_e - u) + \nu \frac{\partial^2 u}{\partial y^2} - \frac{6R_1}{\rho} \left(\frac{\partial u}{\partial y} \right)^2 \frac{\partial^2 u}{\partial y^2} + \frac{4R_2}{\rho} \left[\left(\frac{\partial u}{\partial y} \right) \left(\frac{\partial^2 u}{\partial y^2} \right) \left(u \frac{\partial^2 u}{\partial x \partial y} + v \frac{\partial^2 u}{\partial y^2} \right) + \left(\frac{\partial u}{\partial y} \right)^2 \left(u \frac{\partial^3 u}{\partial x \partial y^2} + v \frac{\partial^3 u}{\partial y^3} + \frac{\partial u}{\partial y} \frac{\partial^2 u}{\partial x \partial y} + \frac{\partial v}{\partial y} \frac{\partial^2 u}{\partial y^2} \right) \right], \tag{2}$$

$$u \frac{\partial T}{\partial x} + v \frac{\partial T}{\partial y} = \alpha \frac{\partial^2 T}{\partial y^2} + \frac{16\sigma^* T_\infty^2}{3k^* \rho c_p} \frac{\partial^2 T}{\partial y^2} - \frac{2\mu R_1}{\rho c_p} \left(\frac{\partial u}{\partial y} \right)^4 + \frac{4\mu R_2}{\rho c_p} u \frac{\partial u}{\partial y} \frac{\partial^2 u}{\partial x \partial y} \left(\frac{\partial u}{\partial y} \right)^2 + \frac{4\mu R_2}{\rho c_p} v \frac{\partial u}{\partial y} \frac{\partial^2 u}{\partial y^2} \left(\frac{\partial u}{\partial y} \right)^2 + \frac{\mu}{\rho c_p} \left(\frac{\partial u}{\partial y} \right)^2 + \frac{\sigma B_0^2 u^2}{\rho c_p} + \tau \left(D_B \frac{\partial C}{\partial y} \frac{\partial T}{\partial y} + \frac{D_T}{T_\infty} \left(\frac{\partial T}{\partial y} \right)^2 \right), \tag{3}$$

$$u \frac{\partial C}{\partial x} + v \frac{\partial C}{\partial y} = D_B \frac{\partial^2 C}{\partial y^2} + \frac{D_T}{T_\infty} \frac{\partial^2 T}{\partial y^2}. \tag{4}$$

The subjected boundary conditions are

$$u = U_w(x) = cx, v = 0, -k \frac{\partial T}{\partial y} = h_1 (T_f - T), -D_B \frac{\partial C}{\partial y} = h_2 (C_f - C) \text{ at } y = 0, u \rightarrow u_e(x) = ax, T \rightarrow T_\infty, C \rightarrow C_\infty \text{ as } y \rightarrow \infty. \tag{5}$$

Here u and v denote the velocity components in the x and y directions respectively, R_1 and R_2 the material constants, σ the electrical conductivity, B_0 the applied magnetic field, ν the kinematic viscosity, ρ the fluid density, μ the fluid dynamic viscosity, k the thermal conductivity, $\alpha = \frac{k}{\rho c_p}$ the thermal diffusivity, T the fluid temperature, T_∞ the ambient temperature, C the fluid concentration, C_∞ the ambient concentration, $u_w(x)$ the stretching velocity, u_e the free stream velocity, σ^* the Stefan–Boltzmann constant, k^* the mean absorption coefficient, $\tau = (\rho c)_p / (\rho c)$ the heat capacity ratio, D_B the Brownian diffusion coefficient, D_T the thermophoresis diffusion coefficient, c_p the specific heat, (h_1, h_2) the wall (heat, mass) transfer coefficient respectively and (T_f, C_f) the convective fluid (temperature, concentration) respectively. Using the transformations

$$\eta = y \sqrt{\frac{c}{\nu}}, u = cx f'(\eta), v = -\sqrt{cx} f''(\eta), \theta(\eta) = \frac{T - T_\infty}{T_f - T_\infty}, \phi(\eta) = \frac{C - C_\infty}{C_f - C_\infty}, \tag{6}$$

the continuity of Eq. (1) is identically satisfied and the resulting problems in f, θ and ϕ are

$$f''' - f'^2 + f f'' + K_1(x) f'^2 f''' + K_2(x) (f' f'^2 f''' + f''^4 - f f'' f''^2 - f f'^2 f''') - Ha^2 (f' - A) + A^2 = 0, \tag{7}$$

$$\left(1 + \frac{4}{3} R \right) \theta'' + Pr f \theta' + Pr Ec f'^2 + \frac{1}{3} K_1 Pr Ec f'^4 + K_2 Pr Ec (f' f'^4 - f f'^3 f''') + Pr Ha^2 Ec f'^2 + Pr Ec f'^2 + Pr N_b \theta' \phi' + Pr N_t \theta^2 = 0, \tag{8}$$

$$\phi'' + Sc f \phi' + \frac{N_t}{N_b} \theta'' = 0, \tag{9}$$

$$f = 0, f' = 1, \theta' = -\gamma_1(1 - \theta(0)), \phi' = -\gamma_2(1 - \phi(0)) \quad \text{at } \eta = 0, \quad (10)$$

$$f' = A, \theta \rightarrow 0, \phi \rightarrow 0 \quad \text{as } \eta \rightarrow \infty.$$

In the above equations K_1 and K_2 are the non-Newtonian parameters, A the ratio of rate constants, Ha^2 the Hartman number, Pr the Prandtl number, N_b the Brownian motion parameter, N_t the thermophoresis parameter, R the radiation parameter, E_c the Eckert number, Sc the Schmidt number, γ_1 the thermal Biot number and γ_2 the concentration Biot number. These quantities are given by

$$K_1 = \frac{-6R_1 c^3 x^2}{\rho \nu^2}, K_2 = \frac{4R_2 c^4 x^2}{\rho \nu^2}, A = \frac{a}{c}, Ha^2 = \frac{\sigma B_0^2}{\rho c},$$

$$Pr = \frac{\nu}{\alpha}, N_b = \frac{\tau D_B (C_f - C_\infty)}{\nu}, N_t = \frac{\tau D_T (T_f - T_\infty)}{T_\infty \nu}, R = \frac{4\sigma^* T_\infty^3}{kk^*}, \quad (11)$$

$$Ec = \frac{u_w^2}{c_p (T_f - T_\infty)}, Sc = \frac{\nu}{D_B}, \gamma_1 = \frac{h_1}{k} \sqrt{\frac{\nu}{\alpha}}, \gamma_2 = \frac{h_2}{D_B} \sqrt{\frac{\nu}{\alpha}}.$$

The skin friction coefficient, local Nusselt and Sherwood numbers are

$$C_f = \frac{\tau_w}{\rho u_w^2}, Nu_x = \frac{xq_w}{k(T_f - T_\infty)}, Sh_x = \frac{xq_m}{D_B(C_f - C_\infty)}, \quad (12)$$

with

$$\tau_w = \mu \left. \frac{\partial u}{\partial y} \right|_{y=0}, \mu|_{y=0} = \mu_0 - 2R_1 \left(\frac{\partial u}{\partial y} \right)^2, \quad (13)$$

$$q_w = - \left(k + \frac{16\sigma^* T_\infty^3}{3k^*} \right) \left(\frac{\partial T}{\partial y} \right)_{y=0}, \quad q_m = -D_B \left(\frac{\partial C}{\partial y} \right)_{y=0}. \quad (14)$$

Dimensionless expressions of skin friction coefficient, local Nusselt and Sherwood numbers are

$$\sqrt{Re_x} C_f = \left(f''(0) + \frac{K_1}{3} (f''(0))^3 \right), \quad (15)$$

$$Nu_x / Re_x^{1/2} = - \left(1 + \frac{4}{3} R \right) \theta'(0), \quad Sh_x / Re_x^{1/2} = -\phi'(0),$$

with $Re_x = u_w(x)/\nu$ as the local Reynolds number.

3. Homotopic solutions

The initial approximations and linear operators are selected as follows:

$$f_0(\eta) = A\eta + (1-A)(1 - e^{-\eta}), \quad \theta_0(\eta) = \frac{\gamma_1}{1 + \gamma_1} e^{-\eta}, \quad \phi_0(\eta) = \frac{\gamma_2}{1 + \gamma_2} e^{-\eta}, \quad (16)$$

$$L_f = f'' - f', \quad L_\theta = \theta'' - \theta, \quad L_\phi = \phi'' - \phi. \quad (17)$$

The above linear operators satisfy the following properties

$$L_f(C_1 + C_2 e^\eta + C_3 e^{-\eta}) = 0, L_\theta(C_4 e^\eta + C_5 e^{-\eta}) = 0, L_\phi(C_6 e^\eta + C_7 e^{-\eta}) = 0, \quad (18)$$

where C_i ($i = 1-7$) indicate the arbitrary constants.

The corresponding problems at the zeroth order are:

$$L_f(C_1 + C_2 e^\eta + C_3 e^{-\eta}) = 0, \quad L_\theta(C_4 e^\eta + C_5 e^{-\eta}) = 0, \quad (19)$$

$$L_\phi(C_6 e^\eta + C_7 e^{-\eta}) = 0,$$

$$(1-p)L_\theta[\hat{\theta}(\eta; p) - \theta_0(\eta)] = p\mathbf{h}_\theta \mathbf{N}_\theta[\hat{f}(\eta; p), \hat{\theta}(\eta; p), \hat{\phi}(\eta; p)], \quad (20)$$

$$(1-p)L_\phi[\hat{\phi}(\eta; p) - \phi_0(\eta)] = p\mathbf{h}_\phi \mathbf{N}_\phi[\hat{f}(\eta; p), \hat{\theta}(\eta; p), \hat{\phi}(\eta; p)], \quad (21)$$

$$\hat{f}(0; p) = 0, \hat{f}'(0; p) = 1, \hat{f}'(\infty; p) = A, \quad (22)$$

$$\hat{\theta}(0; p) = -\gamma_1(1 - \hat{\theta}(0; p)), \hat{\theta}(\infty; p) = 0, \quad (23)$$

$$\hat{\phi}(0; p) = -\gamma_2(1 - \hat{\phi}(0; p)), \hat{\phi}(\infty; p) = 0, \quad (24)$$

$$\mathbf{N}_f[\hat{f}(\eta; p)] = \frac{\partial^3 \hat{f}(\eta; p)}{\partial \eta^3} + (\hat{f}(\eta; p) \frac{\partial^2 \hat{f}(\eta; p)}{\partial \eta^2} - (\frac{\partial \hat{f}(\eta; p)}{\partial \eta})^2)$$

$$+ K_1(x) \left(\frac{\partial^2 \hat{f}(\eta; p)}{\partial \eta^2} \right)^2 \frac{\partial^3 \hat{f}(\eta; p)}{\partial \eta^3}$$

$$+ K_2(x) \left(\frac{\partial \hat{f}(\eta; p)}{\partial \eta} \left(\frac{\partial^2 \hat{f}(\eta; p)}{\partial \eta^2} \right)^2 \frac{\partial^3 \hat{f}(\eta; p)}{\partial \eta^3} + \left(\frac{\partial^2 \hat{f}(\eta; p)}{\partial \eta^2} \right)^4 - \hat{f}(\eta; p) \frac{\partial^2 \hat{f}(\eta; p)}{\partial \eta^2} \left(\frac{\partial^3 \hat{f}(\eta; p)}{\partial \eta^3} \right)^2 \right)$$

$$- \hat{f}(\eta; p) \left(\frac{\partial^2 \hat{f}(\eta; p)}{\partial \eta^2} \right)^2 \frac{\partial^4 \hat{f}(\eta; p)}{\partial \eta^4}$$

$$- Ha^2 \frac{\partial \hat{f}(\eta; p)}{\partial \eta} + Ha^2 A + A^2, \quad (25)$$

$$\mathbf{N}_\theta[\hat{f}(\eta; p), \hat{\theta}(\eta; p), \hat{\phi}(\eta; p)]$$

$$= \left(1 + \frac{4}{3} R \right) \frac{\partial^2 \hat{\theta}(\eta; p)}{\partial \eta^2} + Pr Ec \frac{\partial^2 \hat{f}(\eta; p)}{\partial \eta^2} + Ha^2 Pr Ec \left(\frac{\partial \hat{f}(\eta; p)}{\partial \eta} \right)^2$$

$$+ \frac{1}{3} K_1(x) Pr Ec \left(\frac{\partial^2 \hat{f}(\eta; p)}{\partial \eta^2} \right)^4$$

$$+ K_2(x) Pr Ec \left(\frac{\partial \hat{f}(\eta; p)}{\partial \eta} \left(\frac{\partial^2 \hat{f}(\eta; p)}{\partial \eta^2} \right)^4 - \hat{f}(\eta; p) \frac{\partial^3 \hat{f}(\eta; p)}{\partial \eta^3} \left(\frac{\partial^2 \hat{f}(\eta; p)}{\partial \eta^2} \right)^3 \right)$$

$$+ Pr N_b \frac{\partial \hat{\theta}(\eta; p)}{\partial \eta} \frac{\partial \hat{\phi}(\eta; p)}{\partial \eta} + Pr N_t \frac{\partial^2 \hat{\theta}(\eta; p)}{\partial \eta^2}$$

$$+ Pr Ec \left(\frac{\partial^2 \hat{f}(\eta; p)}{\partial \eta^2} \right)^2 + Pr Ec Ha^2 \left(\frac{\partial \hat{f}(\eta; p)}{\partial \eta} \right)^2, \quad (26)$$

$$\mathbf{N}_\phi[f(\eta; p), \theta(\eta; p), \phi(\eta; p)] = \frac{\partial^2 \phi(\eta; p)}{\partial \eta^2} + Sc f(\eta; p) \frac{\partial \phi(\eta; p)}{\partial \eta} + \frac{N_t}{N_b} \frac{\partial^2 \theta(\eta; p)}{\partial \eta^2}. \quad (27)$$

Here $p \in [0, 1]$ is an embedding parameter and \mathbf{N}_f , \mathbf{N}_θ and \mathbf{N}_ϕ the non-linear operators.

The general solutions (f_m, θ_m, ϕ_m) in terms of special solutions ($f_m^*, \theta_m^*, \phi_m^*$) are

$$f_m(\eta) = f_m^*(\eta) + C_1 + C_2 e^\eta + C_3 e^{-\eta}, \quad (28)$$

$$\theta_m(\eta) = \theta_m^*(\eta) + C_4 e^\eta + C_5 e^{-\eta}, \quad (29)$$

$$\phi_m(\eta) = \phi_m^*(\eta) + C_6 e^\eta + C_7 e^{-\eta}. \quad (30)$$

3.1. Convergence of the developed solutions

Convergence of the developed solutions for the nonlinear differential systems is necessary. For this purpose the h -curves are displayed for the 12th order of approximation in Fig. 1. Permissible values for the derived solutions are found in the ranges $-1.05 \leq h_f \leq -0.45$, $-1.25 \leq h_\theta \leq -0.5$ and $-1.25 \leq h_\phi \leq -0.22$.

3.2. Analysis

The aim of this subsection is to analyze the behaviour of various parameters on the velocity, temperature and concentration distributions.

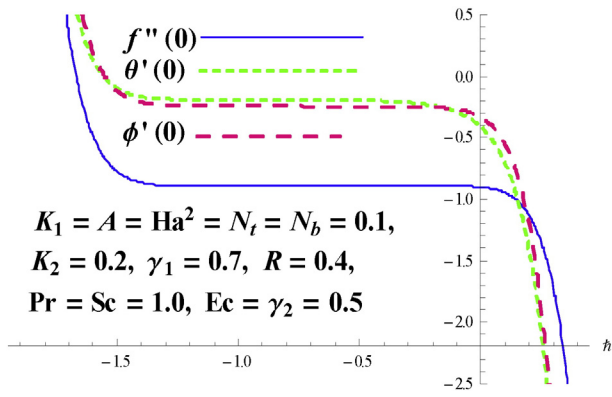


Fig. 1. Curves for the functions f, θ and ϕ .

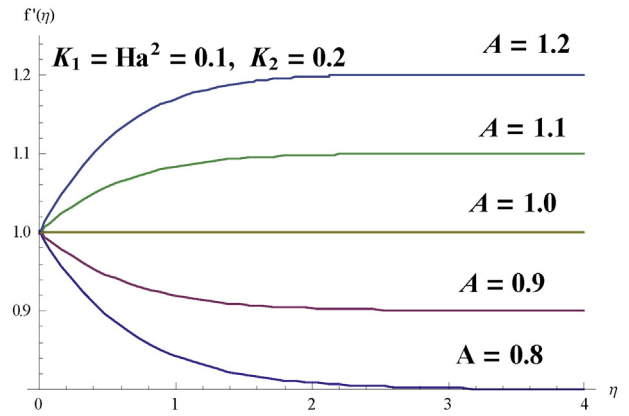


Fig. 4. Impact of A on f' .

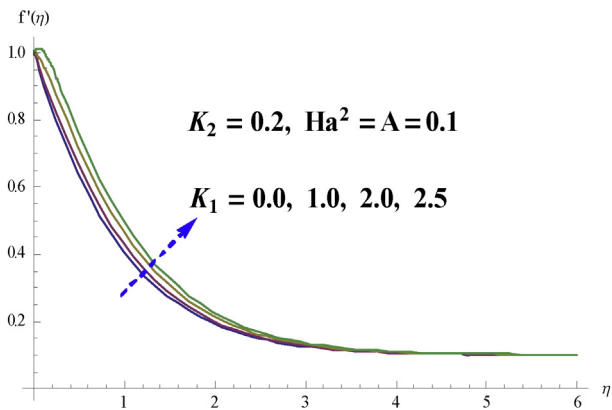


Fig. 2. Impact of K_1 on f' .

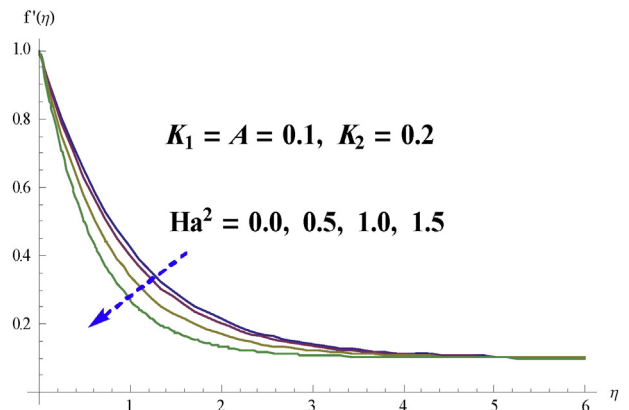


Fig. 5. Impact of Ha^2 on f' .

Figs. 2 and 3 describe the effects of thixotropic parameters K_1 and K_2 on the velocity profile f . It is observed from these plots that K_1 and K_2 cause an increase in fluid velocity. Physically K_1 and K_2 are the thixotropic parameters (having the shear thinning properties which show time-dependent change in viscosity). The longer the fluid undergoes the shear stress causes the reduction in the viscosity finally results into an increase in the velocity of the fluid. Fig. 4 is plotted to see the influence of ratio of rates on velocity profile. It is concluded that velocity profile increases for larger A . Boundary layer thickness increases for $A < 1$ because rate of stretching dominates the rate of free stream. For $A > 1$ i.e. the rate of free stream velocity is greater than the rate of stretching velocity. Here the boundary layer thickness decreases while the velocity distribution increases. It is also observed that there is no boundary

layer for $A = 1$. Variation of the Hartman number Ha^2 on velocity distribution is shown in Fig. 5. Both velocity and momentum boundary layer thickness are reduced for larger Ha^2 . Physically with an increase in Hartman number, the Lorentz force increases and thus the velocity of fluid decreases. Fig. 6 illustrates the influence of Pr on temperature profile $\theta(\eta)$. It is observed that the temperature profile decreases by increasing Pr . It is noticed that both the temperature and thermal boundary layer thickness are decreasing functions of Pr . In fact when Pr increases then thermal diffusivity decreases. This indicates reduction in energy transfer ability and ultimately it results in the decrease of thermal boundary layer. Influences of thermophoresis parameter N_t and Brownian motion parameter on the temperature are observed in Fig. 7. Temperature profile enhances for larger N_t and N_b . This is due to

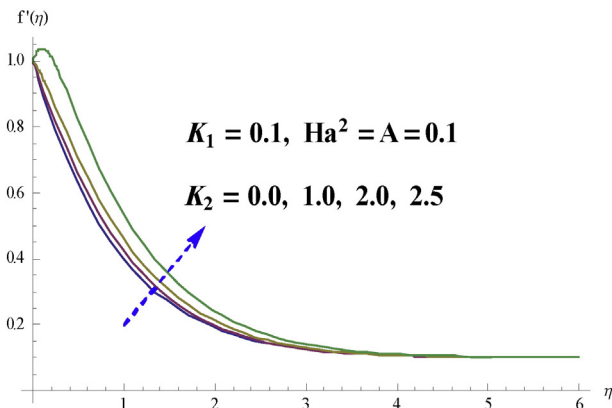


Fig. 3. Impact of K_2 on f' .

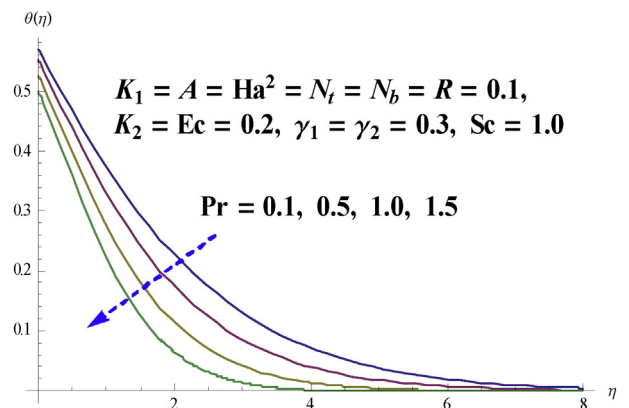


Fig. 6. Impact of Pr on θ .

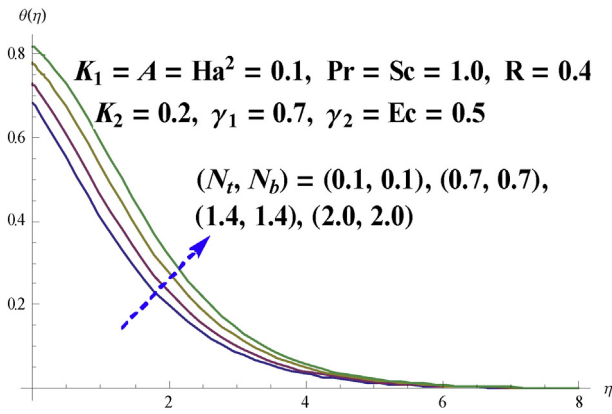


Fig. 7. Impacts of N_t and N_b on θ .

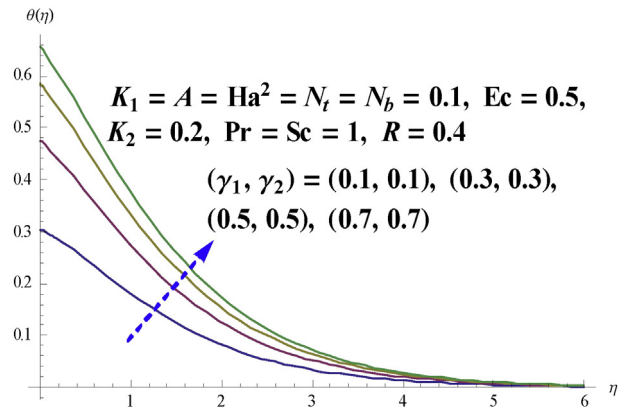


Fig. 10. Impacts of γ_1 and γ_2 on θ .

the fact that when N_t is increased then difference between the wall temperature and reference temperature increases. It causes an increase in temperature while with an increase of the Brownian motion parameter N_b the random motion of particle increases which results in an enhancement of temperature. Characteristics of Eckert number Ec on temperature profile is observed in Fig. 8. It is found that the temperature and thermal boundary layer thickness increase for larger Ec . With the increase of Ec the heat energy is stored in the fluid due to friction forces which enhances the temperature profile. Fig. 9 depicts the influence of radiation parameter R on temperature profile $\theta(\eta)$. Here temperature distribution is increasing function of radiation parameter R . Physically

an increase in thermal radiation parameter reduces the mean absorption coefficient which enhances temperature. Fig. 10 is sketched to see the impacts of γ_1 and γ_2 on temperature profile. It is examined that temperature and associated thermal boundary layer thickness are enhanced for higher values of γ_1 and γ_2 . Analysis of thermophoresis parameter N_t on concentration profile is shown in Fig. 11. It is noted that both the boundary layer and concentration profile $\phi(\eta)$ are increasing functions of N_t . The presence of nanoparticles enhances the thermal conductivity of fluid. An increase in N_t gives rise to the thermal conductivity of fluid. Such higher thermal conductivity shows larger concentration. Effects of Brownian parameter N_b on the concentration profile $\phi(\eta)$ is illustrated

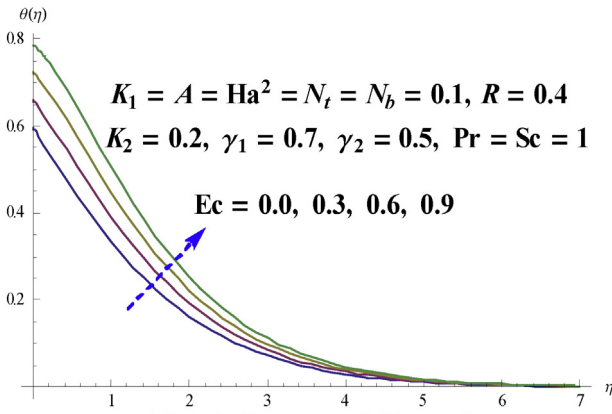


Fig. 8: Impact of Ec on θ

Fig. 8. Impact of Ec on θ .

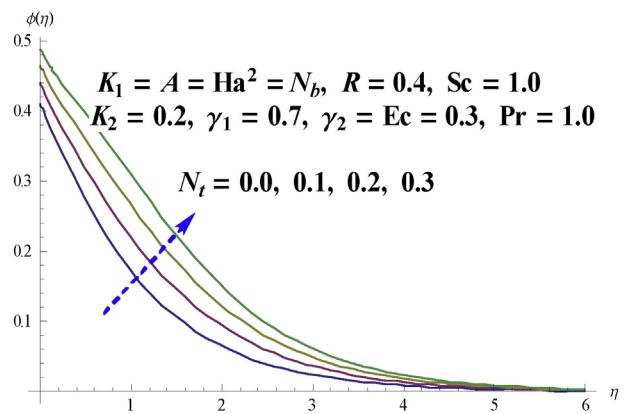


Fig. 11. Impact of N_t on ϕ .

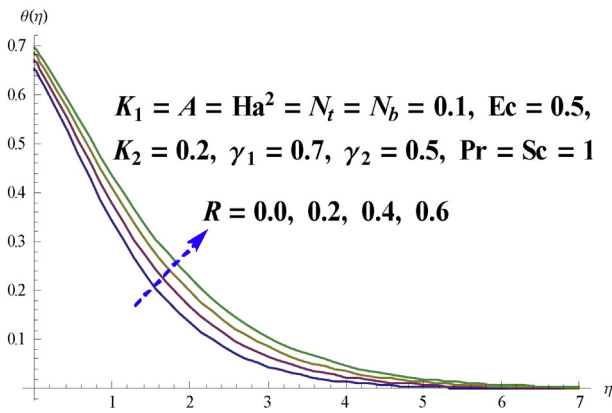


Fig. 9. Impact of R on θ .

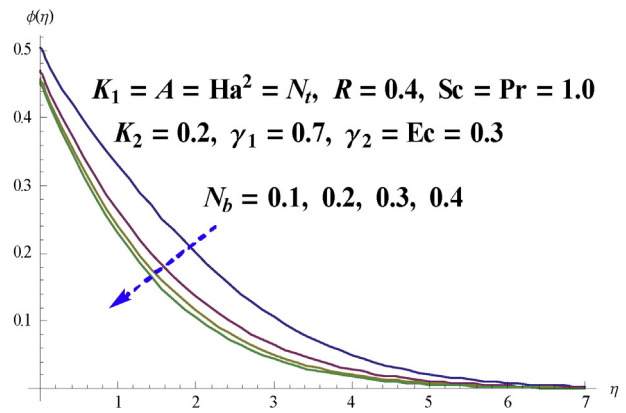


Fig. 12. Impact of N_b on ϕ .

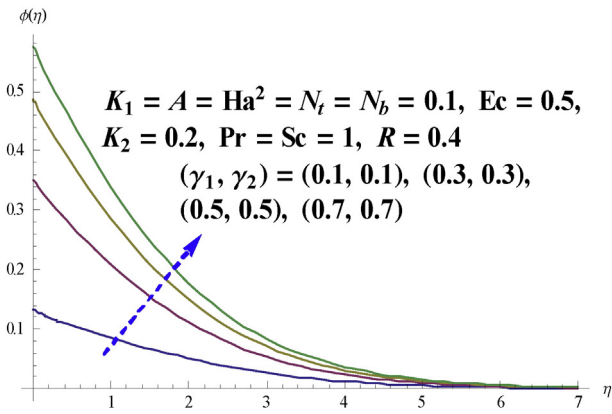


Fig. 13. Impacts of γ_1 and γ_2 on ϕ .

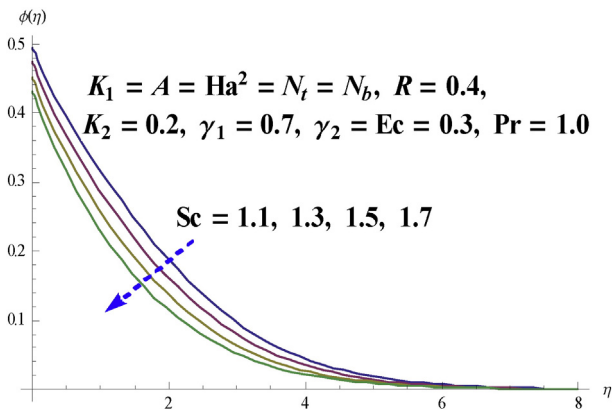


Fig. 14. Impact of Sc on ϕ .

in Fig. 12. It is exposed that as N_b increases the collision between the fluid particles results in decrease of concentration and associated layer thickness. Fig. 13 is presented to see the characteristics of γ_1 and γ_2 on concentration. It is analyzed that concentration and its associated boundary layer enhances for larger values of γ_1 and γ_2 . Fig. 14 portrays the influence of Schmidt number Sc on the concentration profile $\phi(\eta)$. Since Sc is the ratio of momentum to mass diffusivities so an increase in Sc leads to a decrease in mass diffusivity which caused a reduction in concentration $\phi(\eta)$.

Table 1 shows the convergence of the series solutions. It is analyzed that momentum equation converges at 10th order of approximations while temperature and concentration equations converge at 17th and 20th orders of approximations respectively. Table 2 presents the impact of various physical parameters on skin friction coefficient. It is demonstrated that skin friction coefficient increases for larger Ha^2 . However

Table 1

Convergence of series solutions for different orders of approximations when $K_2 = 0.2$, $K_1 = A = Ha^2 = N_t = N_b = 0.1$, $Ec = \gamma_2 = 0.5$, $Pr = Sc = 1.0$, $\gamma_1 = 0.7$ and $R = 0.4$.

Order of approximations	$-f''(0)$	$-\theta'(0)$	$-\phi'(0)$
1	0.8862	0.2779	0.2495
5	0.8934	0.2003	0.2471
10	0.8934	0.1911	0.2429
15	0.8934	0.1899	0.2418
17	0.8934	0.1899	0.2417
20	0.8934	0.1899	0.2417
30	0.8934	0.1899	0.2417
40	0.8934	0.1899	0.2417
50	0.8934	0.1899	0.2417

Table 2

Numerical values of skin friction coefficient for various values of parameters when $N_t = N_b = 0.1$, $Ec = \gamma_2 = 0.5$, $Pr = Sc = 1.0$, $\gamma_1 = 0.7$ and $R = 0.4$.

K_1	K_2	A	Ha^2	$\sqrt{Re_x} C_f$
0.0	0.1	0.2	0.1	-0.9062
0.2				-0.8588
0.4				-0.8183
0.1	0.0			-0.9388
	0.1			-0.9072
	0.2			-0.8815
	0.1	0.0		-0.9047
		0.2		-0.8423
		0.4		-0.7199
		0.1	0.0	-0.8784
			0.2	-0.8907
			0.4	-0.9261

Table 2 shows decreasing behaviours for A , k_1 and K_2 . Features of several parameters of interest on Nusselt number are studied in Table 3. Tabulated values clearly indicate that the Nusselt number enhances for larger Pr , γ_1 and R while it decreases via N_t , N_b , Ec and Ha^2 . Analysis of several

Table 3

Impacts of Pr , N_t , N_b , γ_1 , Ec , Ha^2 and R on Nusselt number when $K_1 = A = 0.1$, $K_2 = 0.2$, $\gamma_2 = 0.5$ and $Sc = 1.0$.

Pr	N_t	N_b	γ_1	Ec	Ha^2	R	$Nu_x Re_x^{-1/2}$
1.2	0.1	0.1	0.7	0.5	0.1	0.4	0.3051
1.4							0.3154
1.6							0.3235
1.0	0.0						0.2971
	0.2						0.2862
	0.4						0.2759
	0.1	0.2					0.2872
		0.4					0.2772
		0.6					0.2684
		0.1	0.4				0.2265
			0.5				0.2527
			0.6				0.2611
			0.7	0.6			0.2665
			0.7	0.7			0.2411
			0.8	0.8			0.2159
				0.5	0.0		0.2942
					0.2		0.2843
					0.4		0.2542
					0.1	0.6	0.3271
						0.7	0.3438
						0.8	0.3600

Table 4

Impacts of Pr , N_t , N_b , γ_2 , Ec and Sc on Sherwood number when $K_1 = A = Ha^2 = 0.1$, $K_2 = 0.2$, $\gamma_1 = 0.7$ and $R = 0.4$.

Pr	N_t	N_b	γ_2	Ec	Sc	$Sh_x Re_x^{-1/2}$
1.2	0.1	0.1	0.5	0.5	1.0	0.2412
1.4						0.2401
1.6						0.2392
1.0	0.0					0.2745
	0.2					0.2120
	0.4					0.1602
	0.1	0.2				0.2590
		0.4				0.2673
		0.6				0.2702
		0.1	0.4			0.2125
			0.6			0.2663
			0.8			0.3051
			0.5	0.6		0.2500
				0.7		0.2578
				0.8		0.2657
				0.5	0.6	0.1871
					0.7	0.2040
					0.8	0.2183

parameters on Sherwood number is presented in Table 4. As expected the value of Sherwood number increases for larger N_b , γ_2 , Ec and Sc however it reduces via Pr and N_t .

4. Final remarks

Here effects of viscous dissipation and Joule heating in magnetohydrodynamic (MHD) flow of thixotropic nanofluid past a stretching sheet have been investigated. The main points of the present analysis are listed below:

- Impacts of K_1 and K_2 on velocity f' are similar.
- Magnetic field corresponds to lower velocity and weaker momentum boundary layer thickness.
- Temperature enhances for larger Eckert number Ec .
- There are similar effects of thermophoresis parameter N_t on temperature and concentration while effects of Brownian motion parameter N_b on temperature and concentration are opposite.
- Concentration boundary layer thickness is thinner for higher values of Schmidt number Sc .

References

- [1] A. Sharma, V.V. Tyagi, C.R. Chen, D. Buddhi, Review on thermal energy storage with phase change materials and applications, *Renew. Sust. Energ. Rev.* 13 (2009) 318–345.
- [2] S.U.S. Choi, Enhancing thermal conductivity of fluids with nanoparticles, *ASME Int. Mech. Eng.* 66 (1995) 99–105.
- [3] C. Zhang, L. Zheng, X. Zhang, G. Chen, MHD flow and radiation heat transfer of nanofluids in porous media with variable surface heat flux and chemical reaction, *Appl. Math. Comput.* 39 (2015) 165–181.
- [4] M. Sheikholeslami, M.G. Bandpy, R. Ellahi, A. Zeeshan, Simulation of MHD CuO–water nanofluid flow and convective heat transfer considering Lorentz forces, *J. Magn. Magn. Mater.* 369 (2014) 69–80.
- [5] S.A. Shehzad, T. Hayat, A. Alsaedi, Influence of convective heat and mass conditions in MHD flow of nanofluid, *Bull. Pol. Ac. Sci. Tech. Sci.* 63 (2015) <http://dx.doi.org/10.1515/bpasts-2015-0053>.
- [6] F.M. Abbasi, S.A. Shehzad, T. Hayat, A. Alsaedi, M.A. Obid, Influence of heat and mass flux conditions in hydromagnetic flow of Jeffrey nanofluid, *AIP Adv.* 5 (2015) 037111.
- [7] M. Sheikholeslami, M. Hatami, G. Domairry, Numerical simulation of two phase unsteady nanofluid flow and heat transfer between parallel plates in presence of time dependent magnetic field, *J. Taiwan Inst. Chem. Eng.* 46 (2015) 43–50.
- [8] U. Farooq, Y.L. Zhao, T. Hayat, A. Alsaedi, S.J. Liao, Application of the HAM-based Mathematica package BVPh 2.0 on MHD Falkner–Skan flow of nanofluid, *Comput. Fluids* 11 (2015) 69–75.
- [9] S.A. Shehzad, T. Hayat, S. Asghar, A. Alsaedi, Stagnation point flow of thixotropic fluid over a stretching sheet with mass transfer and chemical reaction, *J. Appl. Fluid Mech.* 8 (2015) 465–471.
- [10] T. Hayat, S.A. Shehzad, M.B. Ashraf, A. Alsaedi, Magneto-hydrodynamic mixed convection flow of thixotropic fluid with thermophoresis and Joule heating, *J. Thermophys. Heat Transf.* 27 (2013) 733–740.
- [11] S.A. Shehzad, M. Qasim, A. Alsaedi, T. Hayat, M.S. Alhothuali, Combined thermal stratified and thermal radiation effects in mixed-convection flow of a thixotropic fluid, *Eur. Phys. J. Plus* 128 (2013) 7.
- [12] M. Awais, T. Hayat, A. Qayyum, A. Alsaedi, Newtonian heating in flow of thixotropic fluid, *Eur. Phys. J. Plus* 128 (2013) 114.
- [13] Z. Abbas, M. Sheikh, I. Pop, Stagnation-point flow of a hydromagnetic viscous fluid over stretching/shrinking sheet with generalized slip condition in the presence of homogeneous-heterogeneous reactions, *J. Taiwan Inst. Chem. Eng.* 55 (2015) 69–75.
- [14] F. Mabood, W.A. Khan, A.I. Md, Ismail, MHD stagnation point flow and heat transfer impinging on stretching sheet with chemical reaction and transpiration, *Chem. Eng. J.* 273 (2015) 430–437.
- [15] A. Malvandi, F. Hedayati, D.D. Ganji, Slip effects on unsteady stagnation point flow of a nanofluid over a stretching sheet, *Powder Technol.* 253 (2014) 377–384.
- [16] T. Hayat, S. Asad, M. Mustafa, A. Alsaedi, MHD stagnation-point flow of Jeffrey fluid over a convectively heated stretching sheet, *Comput. Fluids* 108 (2015) 179–185.
- [17] K. Bhattacharyya, Heat transfer analysis in unsteady boundary layer stagnation-point flow towards a shrinking/stretching sheet, *Ain Shams Eng. J.* 4 (2013) 259–264.
- [18] B. Sahoo, Effects of slip, viscous dissipation and Joule heating on the MHD flow and heat transfer of a second grade fluid past a radially stretching sheet, *Appl. Math. Mech. Engl. Ed.* 31 (2010) 159–173.
- [19] T. Hayat, M. Waqas, S.A. Shehzad, A. Alsaedi, Effects of Joule heating and thermophoresis on stretched flow with convective boundary conditions, *Scientia Iranica B* 21 (2014) 682–692.
- [20] S.A. Shehzad, A. Alsaedi, T. Hayat, Influence of thermophoresis and Joule heating on the radiative flow of Jeffrey fluid with mixed convection, *Braz. J. Chem. Eng.* 30 (2013) 897–908.
- [21] T. Hayat, A. Shafiq, A. Alsaedi, Effects of Joule heating and thermal radiation in flow of third grade fluid over radiative surface, *PLoS One* 9 (2014), e83153.
- [22] T. Hayat, M. Waqas, S.A. Shehzad, A. Alsaedi, MHD stagnation point flow of Jeffrey fluid by a radially stretching surface with viscous dissipation and Joule heating, *J. Hydrol. Hydromech.* 63 (2015) 311–317.
- [23] M. Turkyilmazoglu, Solution of Thomas–Fermi equation with a convergent approach, *Commun. Nonlinear Sci. Numer. Simul.* 17 (2012) 4097–4103.
- [24] S. Han, L. Zheng, C. Li, X. Zhang, Coupled flow and heat transfer in viscoelastic fluid with Cattaneo–Christov heat flux model, *Appl. Math. Lett.* 38 (2014) 87–93.
- [25] T. Hayat, M. Farooq, A. Alsaedi, Stagnation point flow of carbon nanotubes over stretching cylinder with slip conditions, *Open Phys.* 13 (2015) 188–197.
- [26] M. Sheikholeslami, M. Hatami, D.D. Ganji, Micropolar fluid flow and heat transfer in a permeable channel using analytical method, *J. Mol. Liq.* 194 (2014) 30–36.
- [27] J. Sui, L. Zheng, X. Zhang, G. Chen, Mixed convection heat transfer in power law fluids over a moving conveyor along an inclined plate, *Int. J. Heat Mass Transf.* 85 (2015) 1023–1033.
- [28] S.A. Shehzad, Z. Abdullah, A. Alsaedi, F.M. Abbasi, T. Hayat, Thermally radiative three-dimensional flow of Jeffrey nanofluid with internal heat generation and magnetic field, *J. Magn. Magn. Mater.* 397 (2016) 108–114.
- [29] S. Abbasbandy, T. Hayat, A. Alsaedi, M.M. Rashidi, Numerical and analytical solutions for Falkner–Skan flow of MHD Oldroyd-B fluid, *Int. J. Numer. Methods Heat Fluid Flow* 24 (2014) 390–401.
- [30] T. Hayat, T. Muhammad, S.A. Shehzad, M.S. Alhothuali, J. Lu, Impact of magnetic field in three-dimensional flow of an Oldroyd-B nanofluid, *J. Mol. Liq.* 212 (2015) 272–282.